REMOTE SENSING OF VEGETATION FROM UAV PLATFORMS USING LIGHTWEIGHT MULTISPECTRAL AND THERMAL IMAGING SENSORS

J.A.J. Berni [a], P.J. Zarco-Tejada [a, *], L. Suárez [a], V. González-Dugo [a], E. Fereres [a,b]

[a] Quantalab, Instituto de Agricultura Sostenible (IAS), Consejo Superior de Investigaciones Científicas (CSIC), 14004 Cordoba, Spain - (berni, pzarco, lsuarez, vgonzalez)@ias.csic.es
[b] Dept. of Agronomy, University of Cordoba, Campus Univ. Rabanales, Cordoba, Spain – ag1fecae@uco.es

Inter-Commission WG I/V

ABSTRACT:

Current high spatial resolution satellite sensors lack the spectral resolution required for many quantitative remote sensing applications and, given the limited spectral resolution, they only allow the calculation of a limited number of vegetation indices and remote sensing products. Additionally if short revisit time is required for management applications, the cost of high resolution imagery becomes a limiting factor whereas sensors with shorter revisit time lack the necessary spatial resolution which is critical, particularly for heterogeneous covers. Combining high spatial resolution and quick turnaround times is essential to generate useful remote sensing products for vegetation monitoring applied to agriculture and the environment. Alternatives based on manned airborne platforms provide high spatial resolution and potentially short revisit time, but their use is limited by their high operational complexity and costs.

Remote sensing sensors placed on unmanned aerial vehicles (UAVs) represent an option to fill this gap, providing low-cost approaches to meet the critical requirements of spatial, spectral, and temporal resolutions. However miniaturized electro-optical sensors onboard UAVs require radiometric and geometric calibrations in order to allow further extraction of quantitative results and accurate georeferencing. This paper describes how to generate quantitative remote sensing products using rotating-wing and fixed-wing UAVs equipped with commercial off-the-shell (COTS) thermal and narrowband multispectral imaging sensors. The paper also focuses on the radiometric calibration, atmospheric correction and photogrammetric methods required to obtain accurate remote sensing products that are useful for vegetation monitoring.

During summer of 2007 and 2008, UAV platforms were flown over agricultural fields, obtaining thermal imagery in the 7.5–13-μm region (40 cm spatial resolution) and narrow-band multispectral imagery in the 400–800-nm spectral region (20 cm spatial resolution). Surface reflectance and temperature imagery were obtained, after atmospheric corrections with MODTRAN connected to photogrammetric methods to solve the thermal path length. Biophysical parameters were estimated using vegetation indices, namely, normalized difference vegetation index, transformed chlorophyll absorption in reflectance index/optimized soil-adjusted vegetation index, and photochemical reflectance index (PRI), coupled with PROSPECT, SAILH and FLIGHT models. Based on these parameters, image products of leaf area index, chlorophyll content (Cab), and water stress detection (based on the photochemical reflectance index and on canopy temperature) were produced and successfully validated. GPS/INS data from the autonomous navigation system were used into the aerotriangulation, to georeference the collected imagery, requiring only a minimum number of ground control points. This paper demonstrates that results obtained with a low-cost UAV system for vegetation monitoring applications yield comparable estimations, if not better, than those obtained with more traditional manned airborne sensors.

1. INTRODUCTION

The recent interest of unmanned aerial vehicles (UAV) for vegetation monitoring has been motivated by the benefits of these platforms as compared to full size airborne operation, namely the combination of high spatial resolution and quick turnaround times together with lower operation costs and complexity. These features are of special interest in agriculture where short revisit time is required for management applications and high spatial resolution is mandatory in heterogeneous covers like woody crops. During the last years some UAV based research have been developed for vegetation monitoring on both agricultural and environmental applications.

Large fixed-wing UAVs have been tested for agricultural applications like coffee crops (Herwitz et al. 2004) and vineyards (Johnson et al. 2003). Rotary wing UAVs have also been used for vegetation monitoring in different crops (Suguiura et al, 2005; Berni et al. 2009). Most of these applications have been possible due to the miniaturization of commercial multispectral and thermal cameras which however require radiometric and geometric calibrations together with atmospheric correction and photogrammetric techniques in order to provide image products similar to the available from traditional airborne sensors. The radiometric quality of the images is critical in order to enable the application of quantitative remote sensing methodologies for a successful

---

* Corresponding author.

estimation of biophysical parameters from remote sensing imagery.

This paper describes the aerial platforms and sensors developed for multispectral and thermal image collection but also focuses on the calibration, postprocessing techniques and further validation of remote sensing products obtained using the combination of the images coupled to radiative transfer models.

2. SYSTEM DESCRIPCTION

2.1 Aerial Platforms

Two aerial platforms have been developed based on modified model aircrafts:

 a) *Quanta-H*, is a rotary wing UAV of 1.9 m main rotor diameter and 29 cm^3 gas engine, modified model helicopter (figure 1). This vehicle is capable of carrying 7kg of payload with an endurance of 20m flying at a maximum speed of 30 km/h. The main advantage of this platform is the vertical take off and landing capabilities. However the endurance and speed are a limitation, but make it ideal for small experimental plots.

Figure 1. *Quanta-H* rotary wing UAV with the multispectral camera.

 b) *Quanta-G* is a fixed wing UAV of 3.2m wingspan equipped with a 58 cm^3 gas engine (figure 2). The endurance is 30 minutes flying at 90km/h and the available payload is 5.5kg. Despite the larger yield due to the higher speed and endurance, the main disadvantage is that it requires a runway for take off and landing.

Figure 2. Quanta-G fixed wing UAV.

All these UAV platforms are equipped with an autopilot (Model AP04 UAV Navigation, Spain) which allows fully autonomous navigation following a user-defined flight plan. The autopilot integrates an artificial heading and attitude reference system (AHRS) based on the combination of 3 axis accelerometers and rate gyros, magnetometer, static/dynamic pressure and GPS (a full description is given in Berni et al., 2009). Differential GPS corrections are retrieved from the closest GPS reference station using the NTRIP protocol and uploaded to the UAV through the radio link in order to be applied in real time.

The flight plan is created using a GIS based application that creates a photogrammetric flight plan based on user defined region of interest, flight direction, altitude and focal length of the camera.

2.2 Image Sensors

Two different types of sensors can be installed on the aerial platforms. The multispectral camera (MCA-6, Tetracam Inc., USA) consists on 6 individual sensors and optics with interchangeable optical filters. Sensors features are presented on table 1. The filters are selected depending on the vegetation indices (VI) that are required. Figure 3 shows the band centers and width of some of the narrow band filters used in this study.

Array elements	1280 x 1024
Pixel size	5.2μm x 5.2μm
Image size	6.66mm x 5.32mm
Focal length	8.49 mm
Output	10-bit raw data
S/N Ratio	54 dB
Fixed pattern noise	< 0.03% $V_{PEAK-TO-PEAK}$
Dark current	28mV/s
Dynamic range	60 dB
Total weight	2.7 kg

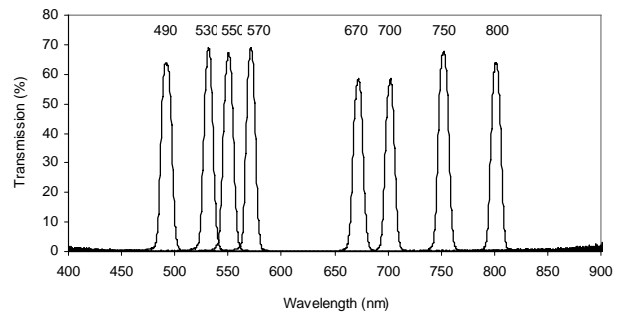Table 1. Technical facts of the multispectral sensors

Figure 3. Spectral characteristics of some of the filters used on the multispectral camera.

The thermal camera installed is a Thermovision A40M (FLIR, USA) equipped with a 40º field-of-view lens. The image sensor is a Focal Plane Array (FPA) based on uncooled microbolometers with a resolution of 320x240 pixels and spectral response in the range 7.5-13 μm (Table 2). The camera delivers digital raw images at 16 bits of at-sensor calibrated radiance with a dynamic rage of 233 K – 393 K. The raw images are stored onboard on a PC104 embedded computer (Cool Little Runner 2, LiPPERT, Germany).

Array Elements	320 x 240
Pixel size	38μm x 38μm
Spectral response	7.5-13μm
Sensibility	0.08K at 303K
Dynamic Range	233K- 393K
Total weight	1.7 kg

Table 2. Technical facts of the thermal sensor

3. INSTRUMENTS CALIBRATION

3.1 Radiometric calibration and atmospheric correction

All the cameras have been calibrated in the laboratory following different approaches depending on the type of sensor. In the case of the multispectral camera, a uniform light source consisting on a 50 cm integrating sphere (Model USS-2000C, Labsphere, USA) is used to calibrate the camera to radiance. In order to convert the radiance images to reflectance, the SMARTS irradiance model (Gueymard, 2001) is used to simulate ground surface irradiance. A sun photometer (Microtops, Solar Inc, USA) is used to retrieve aerosol optical depth at 6 different wavelength and total water content, which are the inputs to the irradiance model.
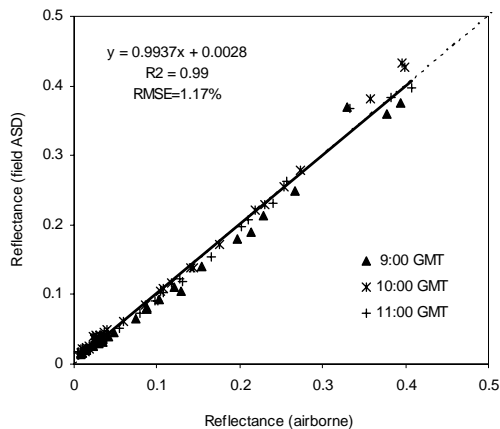
Figure 4. Field validation of the reflectance. The plot shows 90 points from 3 flights over 5 targets for 6 spectral bands.

In the case of the thermal camera, laboratory calibration was conducted using a calibration blackbody source (RAYBB400, Raytek, CA, USA). In order to apply an atmospheric correction, the MODTRAN radiative transfer code (Berk et al., 1999) is used to model the atmospheric transmissivity and longwave thermal path radiance. Since only vegetation temperature is retrieved, surface emissivity is considered as 0.98 as an accepted value for natural vegetation. Local atmospheric conditions such as air temperature, relative humidity and barometric pressure are measured at the time of flight with a portable weather station (Model WXT510, Vaisala, Finland) and used as input into MODTRAN model. Both, path transmittance and thermal radiance are simulated at different sensor altitudes and integrated for the spectral response range of the thermal camera. The validation was conducted flying at 3 different times during one diurnal course and over three

different surfaces (see Berni et al., 2009) and showed that the errors for not accounting for the atmospheric effects are higher than 3 K, which are reduced to errors below 1K after the atmospheric correction (figure 5).
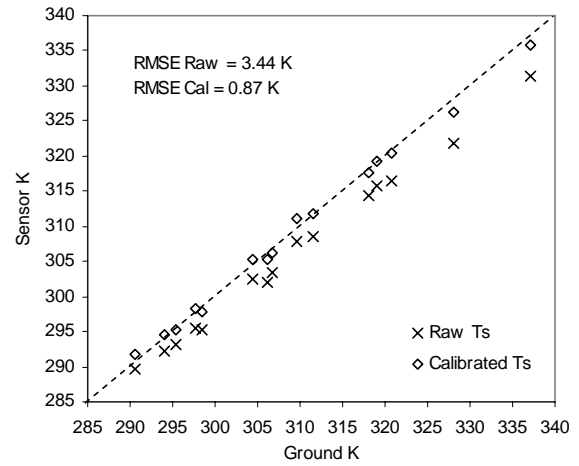
Figure 5. Comparison between ground truth surface temperature (IRT measured) and obtained from the thermal camera at 150 m flight altitude before (×) and after (○) applying the atmospheric correction

3.2 Geometric calibration

The geometric calibration of the cameras has been performed using Bouguet's camera calibration toolbox (Bouguet, 2001). This methodology consists on placing a calibration checkerboard pattern on a fixed location and acquiring several images from different locations and orientations. The grid corner coordinates were extracted semiautomatically from the images, and the intrinsic parameters and exterior orientation (EO) were calculated. In the case of the thermal camera, a calibration pattern was built using resistive wires to obtain a bright pattern when electricity circulated through the wires, thus increasing their temperature. The results of the calibration are the internal parameters of the camera (focal length and principal point coordinates) and a distortion map (figure 6) that can be used to estimate the distortion coefficients for any photogrammetric software.
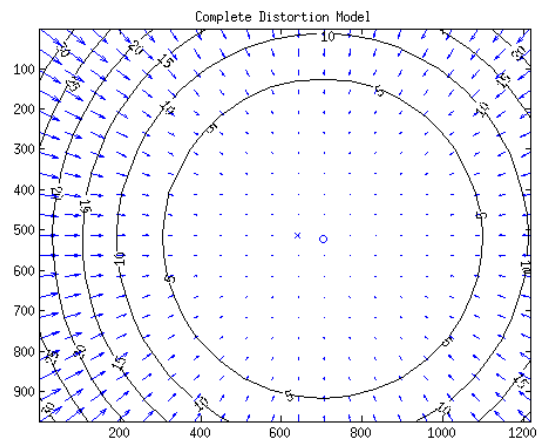
Figure 6. Distortion map generated with the geometric calibration procedure.

4. IMAGE PRODUCTS

4.1 Photogrammetric workflow

The INS/GPS data from the autopilot at the exact time of image acquisition is used to filter out the images acquired during turns and outside the region of interest, as well as images with excessive roll. The exterior orientation (EO) is used also as an initial approximation for the aerotriangulation (AT). In order to provide a good synchronization of the autopilot data (UTC time) and the image acquisition, a second GPS (model Copernicus, Trimble, USA) was used as time source. The image trigger was captured together to the UTC time from the auxiliary GPS receiver using a dedicated microcontroller. The pulse per second (PPS) signal from the GPS was used to ensure time accuracies better than 10ms.

Automatic tie points are extracted using the SIFT algorithm (Lowe, 2004) and self made software. This algorithm has shown very robust results as compared with automatic tie point extraction with other photogrammetric software.

The images are loaded together with the auxiliary data into the Leica Photogrammetric Suite (LPS, Leica Geosystems, Switzerland), where uniformly-distributed ground control points (GCP) were measured throughout the block. Once the model definition is complete it is possible to run the triangulation adjusting the weight assigned to EO, GCP and image measurements. When the AT is accepted it is possible to create the orthomosaic from the images using ready available high spatial resolution DEM. At present, orthomosaics of 600 images have been successfully generated following this methodology (figure 7).
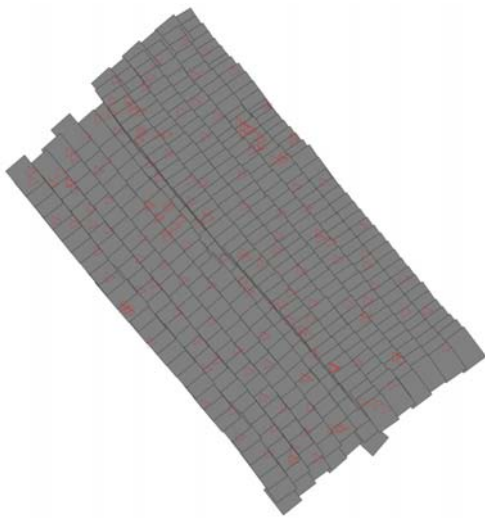

Figure 7. Example of a photogrammetric block of 423 images showing the ground control points with red triangles.

4.2 Parameter estimation from vegetation indexes

Several airborne and field campaigns were performed with the multispectral camera using the six 10nm FWHM bands. The average flight height was 150 m yielding 20 cm ground resolution imagery. The Normalized Difference Vegetation Index (NDVI) (Rouse et al., 1974) was calculated to assess the estimation of crown leaf area index (cLAI) over a variety field of olive trees (figure 8a). Using an empirical relationship obtained by field measurements of cLAI showed good agreement (r^2=0.88, $RMSE$=0.13), allowing to map the field variability of cLAI for the different olive varieties (figure 8b).
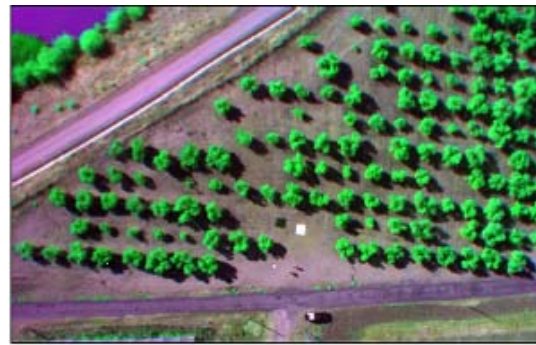
a)
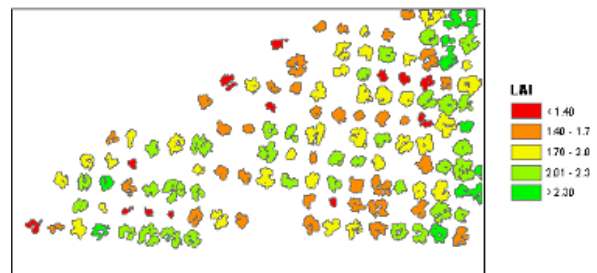
b)

Figure 8. Estimation of tree LAI over a variety field of olive trees: a) false colour composite of the study site; b) crown LAI estimated for each individual tree.

The Transformed Chlorophyll Absorption in Reflectance Index (TCARI) (Haboudane, 2002) normalized by the Optimized Soil-Adjusted Vegetation Index (OSAVI) (Rondeaux et al., 1996) to obtain TCARI/OSAVI is demonstrated to successfully minimize soil background and leaf area index variation in crops, providing predictive relationships for chlorophyll concentration estimation with narrow-band imagery in open tree canopy orchards (Zarco-Tejada et al., 2004). The leaf-level radiative transfer model PROSPECT (Jacquemoud & Baret, 1990) was linked with the canopy-level Forest LIGHT Interaction Model (FLIGHT) (North, 1996) and SAILH (Verhoef, 1984) to obtain predicting algorithms for chlorophyll concentration (Cab) from the airborne TCARI/OSAVI index. The comparison between field measured Cab in olive trees at the same variety field and airborne-estimated Cab yielded a $RMSE$ of 4.2 μg/cm2 and r^2=0.89 (Berni et al., 2009) showing the capabilities of this system for estimating chlorophyll content at the crown level.
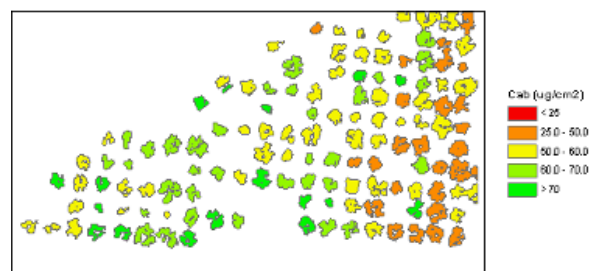

Figure 9. Estimation of chlorophyll content for individual trees over a variety field of olive trees.

The Photochemical Reflectance Index (PRI) (Gamon et al., 1992) was calculated to assess its potential capability for water stress detection from the UAV platform. The PRI index was calculated with the MCA-6 camera using additional 10 nm FWHM filters centered at 530 and 570 nm wavelengths. A flight was conducted over an experimental field of olive trees with deficit irrigation treatments (see Suárez et al., 2009). Water stress levels were quantified by comparing the image-derived PRI and the simulated non-stress PRI (sPRI) obtained through radiative transfer. PRI simulation was conducted using PROSPECT-FLIGHT and PROSPECT-SAILH radiate transfer models. The PRI values of the deficit irrigation treatments (figure 10) were consistently higher than the modelled PRI for the study sites, correlating well with tree xylem water potential (r^2=0.84), thus enabling the identification of individual water-stressed trees.
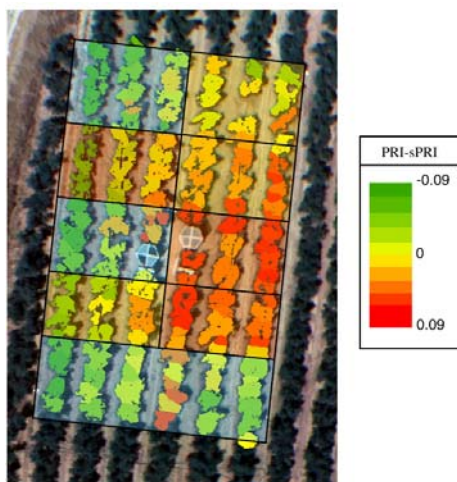

Figure 10. Crown PRI minus simulated PRI (PRI−sPRI) map over olive trees with different irrigation treatments.

Finally, thermal imagery of 40 cm spatial resolution was acquired over the same experimental field used for PRI validation (figure 11). The high spatial resolution allows isolating the tree crowns temperature from the soil and shadows enabling the retrieval of vegetation temperature. Canopy temperature yielded a relationship with water potential of r^2=0.82 which suggest that this can be a valuable tool to track water stress on heterogeneous crops.
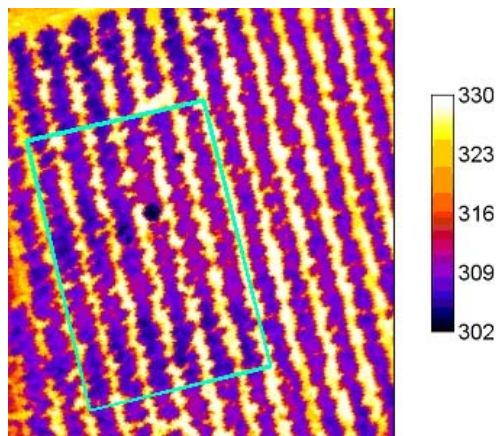

Figure 11. Surface temperature image over olive trees with different irrigation treatments.

5. CONCLUSIONS AND OUTLOOK

This work demonstrated that it is possible to generate quantitative remote sensing products by means of a UAV equipped with commercial off-the-shelf (COTS) thermal and multispectral imaging sensors. Laboratory and field calibration methods provided 6-band 10 nm FWHM multispectral imagery with RMSE of 1.17% in ground reflectance and less that 0.2m spatial resolution. For the thermal camera, atmospheric correction methods based on MODTRAN radiative transfer model showed the successful estimation of surface temperature images of 40 cm spatial resolution, yielding RMSE < 1 K.

Photogrammetric techniques were required to register the frame-based imagery to map coordinates. Cameras were geometrically characterized with their intrinsic parameters. These techniques along with position and attitude data gathered from the autopilot enabled the generation of large mosaics semi-automatically with minimum use of ground control points.

Appropriate bandset configurations selected for the multispectral camera enabled the calculation of several traditional narrowband vegetation indices (NDVI, TCARI/OSAVI and PRI), which were linked to biophysical parameters using quantitative methods based on physical approaches such as PROSPECT, SAILH, and FLIGHT models.

The high spatial, spectral and temporal resolution provided at high turnaround times, make this platform particularly suitable for a number of applications, including precision farming or irrigation scheduling, where time-critical management is required.

REFERENCES

Berk, A.; Anderson, G.; Acharya, P.; Chetwynd, J.; Bernstein, L.; Shettle, E.; Matthew, M.; Adler-Golden, S. (1999) Modtran4 user's manual.

Berni, J.; Zarco-Tejada, P.; Suarez, L.; Fererez, E. (2009) Thermal and narrow-band multispectral remote sensing for vegetation monitoring from an unmanned aerial vehicle. *IEEE Transactions On Geoscience And Remote Sensing*, 47, 722-738.

Bouguet, J. (2001) Camera calibration toolbox for matlab. http://www.vision.caltech.edu/bouguetj/calib_doc/ (accessed 15 Apr. 2009)

Gamon, J.; Penuelas, J.; Field, C. (1992) A narrow-waveband spectral index that tracks diurnal changes in potosynthetic efficiency. *Remote Sensing of Environment*, 41, 35-44.

Haboudane, D. and Miller, J. R. and Tremblay, N. and Zarco-Tejada, P. J. and Dextraze, L. (2002) Integrated narrow-band vegetation indices for prediction of crop chlorophyll content for application to precision agriculture. *Remote Sensing Of Environment*, 81, 416-426.

Jacquemoud, S.; Baret, F. (1990) Prospect: a model of leaf optical properties spectra. *Remote Sensing of Environment*, 34, 75-91.

Lowe, D. (2004) Distinctive image features from scale-invariant keypoints. *Int. J. Comput. Vis.*, 60, 91-110.

North, P.R.J. (1996) Three-dimensional forest light interaction model using a montecarlo method. *IEEE Transactions on Geosciences and Remote Sensing*, 34, 946-956.

Rondeaux, G.; Steven, M.; Baret, F. (1996) Optimization of soil-adjusted vegetation indices. *Remote Sensing of Environment*, 55(2), 95−107.

Rouse JW, Haas RH, Schell JA, Deering DW, Harlan JC (1974) Monitoring the vernal advancements and retrogradation of natural vegetation. In: MD UG, editor. NASA/GSFS final report. . p. 371.

Suárez, L.; Zarco-Tejada, P.; Berni, J.; González-Dugo, V.; Fereres, E. (2009) Modelling PRI for water stress detection using radiative transfer models. *Remote Sensing of Environment*, 113, 730-744.

Verhoef, W. (1984) Light scattering by leaf layers with application to canopy reflectance modeling: the sail model. *Remote Sensing of Environment*, 16, 125-141.

Zarco-Tejada, P.; Miller, J.; Morales, A.; Berjon, A.; Aguera, J. (2004) Hyperspectral indices and model simulation for chlorophyll estimation in open-canopy tree crops. *Remote Sensing Of Environment*, 90, 476.